Available online at www.sciencedirect.com
SCIENCE DIRECT®
International Journal of Heat and Mass Transfer 47 (2004) 3085–3095
International Journal of HEAT and MASS TRANSFER
www.elsevier.com/locate/ijhmt

Joule heating effects in electroosmotically driven microchannel flows

Keisuke Horiuchi, Prashanta Dutta *

Mechanical and Materials Engineering, Washington State University, Pullman, WA 99164-2920, USA

Received 26 September 2003; received in revised form 23 February 2004

Abstract

Analytical solutions for temperature distributions, heat transfer coefficients, and Nusselt numbers of steady electroosmotic flows are obtained for two-dimensional straight microchannels. This analysis is based on an infinitesimal electric double layer in which flow velocity becomes "plug-like", except very close to the wall. Both constant surface temperature and constant surface heat flux conditions are considered in this study. Separation of variables technique is applied to obtain analytical solutions of temperature distributions from the energy equation of electroosmotically driven flows. The thermal analysis considers interaction among inertial, diffusive and Joule heating terms in order to obtain thermally developing behavior of electroosmotic flows. Heat transfer characteristics are presented for low Reynolds number microflows where the viscous and electric field terms are very dominant. For the parameter range studied here ($Re \leqslant 0.7$), the Nusselt number is independent of the thermal Peclet number, except in the thermally developing region. Analytical results for cases with and without Joule heating are also compared with the existing heat transfer results, and an excellent agreement is obtained between them.

Keywords: Microfluidics; Electroosmotic flow; Joule heating

1. Introduction

Electroosmosis, one of the main electrokinetic effects, is the process by which an ionized liquid moves with respect to a stationary charged surface under the action of an external electric field. The electroosmotic phenomenon was first observed by Ruess in 1809 from an experimental study on clay diaphragms [1]. In the mid-19th century, Wiedemann repeated the experiment and formally introduced the mathematical theory behind it [2]. Though the electroosmotic phenomenon has been known for more than a century, the application of electroosmotic flow was only limited in the field of analytical chemistry to transport samples in capillaries. But, recent developments in microelectronics and micro-electro-mechanical systems (MEMS) have made a breakthrough progress toward utilizing electroosmotic flows in complex microfluidic networks for "lab-on-a-chip" applications. Lately, scientists at Sandia National Lab [3] and Stanford University [4,5] have successfully developed electrokinetic micropumps capable of creating in excess of 20 atm by packing micron sized non-porous silica particles in a 500–900 μm diameter fused silica capillary. Due to the ability of pumping a wide range of working fluid, this non-mechanical pumping has become an attractive fluid handling method in the emerging "lab-on-a-chip" microfluidic devices for sample loading, mixing, flushing and reagent transporting [6,7]. So far, most of the studies have been focused only on the fluid flow behavior where the velocity distribution is plug like in most of the channel [8–12], and not much attention has been paid on the thermal behavior.

One of the main objectives of electroosmotic action is to generate pressure head for pumping liquid in microfluidic devices for bioanalytical applications. Here the

* Corresponding author. Tel.: +1-509-335-7989; fax: +1-509-335-4662.
E-mail address: dutta@mail.wsu.edu (P. Dutta).

0017-9310/$ - see front matter © 2004 Elsevier Ltd. All rights reserved.
doi:10.1016/j.ijheatmasstransfer.2004.02.020

Nomenclature

A_C	cross-sectional area of a microchannel [m^2]
c_p	specific heat at constant pressure [J/(kg K)]
D	half channel height [m]
D_H	hydraulic diameter [m]
$\vec{E}$	applied electric field [V/m]
E_x	electric field component in the streamwise direction [V/m]
e	electron charge [C]
G	non-dimensional generation term
h	local heat transfer coefficient [W/(m^2 K)]
k	thermal conductivity [W/(m K)]
k_B	Boltzmann constant [J/K]
L	channel length [m]
$\dot{m}$	mass-flow rate [kg/s]
n_0	average number of positive/negative ions in the buffer [1/m^3]
Nu	Nusselt number, Dh/k
Pe_T	thermal Peclet number, $Re \cdot Pr$
Pr	Prandtl number, ν/α
q''_s	surface heat flux [W/m^2]
Re	Reynolds number, $u_m D/\nu$
R_{ev}	ratio of Joule heating to viscous dissipation
T	temperature [K]
u	velocity component in the streamwise direction [m/s]
u_{HS}	Helmholtz–Smoluchowski velocity [m/s]
$\vec{V}$	velocity field [m/s]
v	velocity component in the cross-stream direction [m/s]
W	channel width [m]
z	valence

Greek symbols

α	thermal diffusivity, $k/(\rho c_p)$ [m^2/s]
α_n	Fourier coefficient
β_0	Fourier coefficient
β_n	Fourier coefficient
δ_{99}	effective Debye layer thickness [m]
ε	permittivity of the medium [C/(V m)]
Φ	viscous dissipation function
γ_n	exponential decay parameter, $(\sqrt{Pe_T^2 + 4\lambda_n} - Pe_T)/2$
η	non-dimensional cross-stream distance, y/D
λ	Debye length [m]
λ_n	eigenvalues
μ	dynamic viscosity coefficient [N s/m^2]
θ	non-dimensional temperature
θ_a	auxiliary temperature field
θ_p	particular type of function
$\Delta\theta$	non-dimensional temperature difference $\theta_s - \theta$
ρ_f	fluid density [kg/m^3]
ρ_e	electric charge density [C/m^3]
σ	electrical conductivity of the buffer fluid [S/m]
υ	kinetic viscosity [m^2/s]
ξ	non-dimensional streamwise distance x/D
ψ	electrokinetic potential [V]
ζ	zeta potential [V]

Subscripts

c	centerline
h	homogenous
i	inlet
m	mean
o	non-homogenous
s	surface

pumping action can be achieved by applying a very high external electric field along the channel. This high external electric field creates both conduction and convection current in the liquid, where convection current contributes to net flow in the system and conduction current generates volumetric Joule heating in the system [8]. This Joule heating effect is very significant for high electric field strength and/or highly conductive buffer. Since Joule heating is a volumetric phenomenon, its magnitude is directly related to the channel volume. In typical electroosmotic flows with a fluid of 10^{-3} S/m electrical conductivity and an applied electric field of 10 V/mm, the Joule heating term contributes 10^5 W/m^3. Depending on the surface (thermal) conditions, this thermal energy may elevate the system enthalpy significantly [13]. The thermal energy generation and the associated dissipation mechanisms have received very little attention, especially for electroosmotic microflows. However, there are several analytical and experimental works that appeared in literature describing the effect of Joule heating in capillary electrophoresis for identical electric field and ion concentration [14,15]. Those works identified thermal band broadening due to Joule heating.

Explicit analytical solutions have been reported in the past for both developing and fully developed thermal transport problems with or without volumetric heat generation. In a seminal work, Sparrow and co-workers [16] studied the effect of an arbitrary generation term in pressure driven thermally developing flows, and they obtained analytical solutions for heat transfer characteristics. Their framework is very similar to this study, but in our case the hydraulically fully developed electroosmotic (plug like) velocity is used instead of pressure driven parabolic velocity profiles. In literature there also

exist numerous heat transfer studies in the slug flows both in parallel plates and in circular channels [17,18], where they have not considered any Joule heating or generation terms. Recently, Maynes and Webb have presented thermal analysis of electroosmotic flows for circular tubes and parallel plates under Debye Huckel linearization [19]. However, that study is limited only to the fully developed thermal region.

In this article, we obtain analytical solutions for temperature distributions and heat transfer characteristics for thermally developing steady electroosmotic flow in two-dimensional straight microchannels. Our analysis takes care of the interaction among convection, viscous, and Joule heating terms to obtain the temperature distribution of the fluid in microchannels. This analysis identifies the effects of Joule heating during electroosmotic pumping in designing electroosmotically driven micropumps, valves, and mixers where surface can be maintained either at constant temperature or at constant heat flux with the surrounding.

2. Theory

The formation of electroosmotic flow in a straight microchannel is shown in Fig. 1. Here the channel walls attain net negative charges due to ionization, ion absorption, or ion adsorption from the polar liquid next to the solid surface. These trapped surface charges significantly influence the distribution of ions in the liquid side. Due to the presence of negative charges on the surface, positive ions from the solution get attracted to the channel surface, and negative ions get repelled from the surface, forming an electric double layer (EDL) very close to the channel wall. The EDL is typically 1–30 nm thick depending on the concentration of the solutions. For example, ion concentrations of 1 and 100 mM correspond to EDL thickness of 10 and 1 nm, respectively. In the EDL, the ion density of counter-ions is greater than that of co-ions. The electroosmotic microflow occurs when an EDL interacts with the externally applied electric fields. In Fig. 1, the positively charged ions of EDL are attracted towards cathode and repelled by the anode. This results in the net movement of ionized fluid in the direction of the electric field.

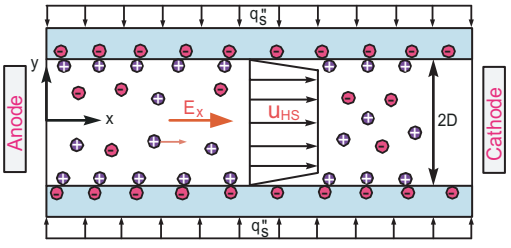

Fig. 1. Schematic view of electroosmotic flow between two parallel plates subjected to constant heat flux boundary conditions at the top and bottom surfaces.

2.1. Governing equations

The steady electroosmotic flow is governed by the modified Navier–Stokes equations as [20]

$$\rho_f(\vec{V}\cdot\nabla)\vec{V} - \mu\nabla^2\vec{V} + \nabla P - \rho_e\vec{E} = 0 \tag{1}$$

where ρ_f is the fluid density, μ is the dynamic viscosity, $\vec{E}$ is the applied electric field, and $\vec{V} = (u, v)$ is the velocity field. The incompressibility condition requires a divergence free velocity field ($\nabla\cdot\vec{V} = 0$), subjected to no slip and no penetration boundary conditions at the surface. The first and second terms of Eq. (1) indicate the inertia and viscous forces, respectively. While the third term shows the pressure force, and the final term, $\rho_e\vec{E}$, represents the electrokinetic body force due to the formation of the EDL next to the surface. Here ρ_e is the electric charge density, and for a symmetric univalent dilute electrolyte it can be found as [20]

$$\rho_e = -2n_0 ez\sinh\left(\frac{ez\psi}{k_B T}\right) \tag{2}$$

where ψ is the electrokinetic potential, n_0 is the average number of positive or negative ions in the buffer, e is the electron charge, z is the valence, k_B is the Boltzmann constant, and T is the absolute temperature. At steady state, the electrokinetic potential, ψ, can be obtained from the Poisson–Boltzmann equation as [21]

$$\nabla^2\psi = -\frac{\rho_e}{\varepsilon} \tag{3}$$

where ε is the permittivity of the medium.

For steady electroosmotic microflow, the governing equation for thermal energy transport can be presented as

$$\rho_f c_p(\vec{V}\cdot\nabla)T - \nabla\cdot(k\nabla T) - \mu\Phi - \sigma(\vec{E}\cdot\vec{E}) = 0 \tag{4}$$

where c_p is the specific heat capacity, T is the temperature, k is the thermal conductivity, Φ is the viscous dissipation, and σ is the electrical conductivity of the buffer fluid. The first and second terms of Eq. (4) indicate the thermal energy transfer due to convection and thermal diffusion, respectively, while the third and fourth terms show thermal energy generation in the system due to viscous dissipation and Joule heating, respectively.

2.2. Assumptions and approximations

The main simplifying assumptions and approximations in our analysis are as follows:

- The fluid viscosity is independent of the shear rate. Hence, we assume a Newtonian fluid.

- The fluid viscosity is independent of the local electric field strength. This condition is an approximation. Since the ion concentration and the electric field strength within the EDL are increased, the viscosity of the fluid may be affected.
- The Poisson–Boltzmann equation is valid when the ion convection effects are negligible. Hence, our analysis is valid for Stokes flows, or for hydraulically fully developed channel flows.
- The solvent is continuous, and its permittivity is not affected by the overall and the local electric field strength.
- The ions are point charges.
- The zeta potential is uniform throughout the channel wall. Hence relatively low temperature variation in the system is assumed.
- Joule heating takes place uniformly throughout the channel.
- Fluid properties are independent of temperature change. This can be justified for smaller temperature change (less than 10 K).
- No pressure driven component is present in the velocity distribution.

2.3. Analysis of pure electroosmotic flow

Electroosmotic flow in microchannels has been extensively studied in the past, and detailed analysis of electroosmotic flow can be obtained from earlier flow studies [8–11]. In this study, we review the necessary parameters for the complete understanding of the electroosmotic phenomena. From experimental studies it has been found that microchannel electroosmotic flow is generally very slow in nature with very low Reynolds number, $Re \ll 1$. Therefore, the inertial term in Eq. (1) is negligible compared to viscous term. Moreover, for pure electroosmotic flow in a 2-D straight microchannel there is no pressure gradient, and hence the electroosmotic body force term is counterbalanced by the viscous term. In a two-dimensional straight channel, the steady electroosmotic velocity distribution becomes [10]

$$u(x,y) = u_{\mathrm{HS}}\left(1 - \frac{\psi}{\zeta}\right) \tag{5}$$

where ζ is the zeta potential and u_{HS} is the Helmholtz–Smoluchowski electroosmotic velocity, which is given by $u_{\mathrm{HS}} = -\varepsilon\zeta E_{\mathrm{x}}/\mu$. For a straight microchannel ($D > 10\lambda$), the electroosmotic potential can be found by solving Eq. (3) as [10]

$$\psi = \frac{4k_{\mathrm{B}}T}{ez}\tanh^{-1}\left[\tanh\left(\frac{ez\zeta}{4k_{\mathrm{B}}T}\right)\exp\left\{\frac{|y|-D}{\lambda}\right\}\right] \tag{6}$$

where λ is the Debye length and D is the half channel height. The electrokinetic and flow parameter ranges studied for this analysis, as presented in Table 1, show that the electrokinetic potential diminishes within the effective Debye layer thickness, δ_{99} ($\delta_{99} \leqslant 5\lambda$). For more information about the EDL, δ_{99}, electrokinetic potential, and electroosmotic velocities, readers are advised to consult classical electroosmotic flow studies by Hunter [21].

Table 1
Typical length scale, electrokinetic and flow parameters considered in this theoretical work

Parameter	Notation (Unit)	Range
Half channel height	D (μm)	10–300
Electrolyte concentration	n_0 (mM)	1–100
Debye length	λ (nm)	3–30
Characteristic length ratio	D/λ	1000–30,000
Axial electric field	E_{x} (V/mm)	1–300
Zeta potential	ζ (mV)	−100 to −25
Reynolds number	Re	0.001–0.700
Peclet number	Pe_{T}	0.001–5.000

It is clear from Eqs. (5) and (6) that electroosmotic flow velocity remains plug-like, except very close to the wall. Therefore in Eq. (4), the viscous dissipation term is only active within the effective EDL, δ_{99}, where local velocity changes from u_{HS} to zero. But, Joule heating due to electric current will take place uniformly over the entire volume. For pure electroosmotic flow in a 2-D straight channel, the ratio of Joule heating to viscous dissipation can be expressed as

$$R_{\mathrm{ev}} = \frac{\sigma E_{\mathrm{x}}^2(2DWL)}{\mu\left(\frac{\partial u}{\partial y}\right)^2(2\delta_{99}WL)} \cong \frac{D\delta_{99}\sigma}{\zeta^2}\frac{\mu}{\varepsilon^2} \tag{7}$$

where W is the channel width and L is the channel length. From Eq. (7), it is clear that the ratio of generation terms, R_{ev}, is independent of the externally applied electric field, but it depends on characteristic dimensions, effective Debye layer thickness, and conductivity. Therefore, for typical electroosmotic flow with $\delta_{99} = 10^{-8}$ m, $\sigma = 10^{-3}$ S/m, $\mu = 10^{-3}$ N s/m^2 and $\zeta = -100$ mV, the Joule heating term is dominating when D is 10 μm or higher. Hence we assume that our channel depth is larger than 20 μm ($D \geqslant 10$ μm), and the viscous dissipation term was neglected for this analysis.

3. Normalized energy equation

We normalize streamwise and cross-stream coordinates (x, y) with the half channel height D ($\xi = x/D$, $\eta = y/D$). Here, D is used as the characteristic length as opposed to hydraulic diameter, D_{H} ($D_{\mathrm{H}} = 4D$). Hence the flow Reynolds and Nusselt numbers in this study will be one fourth of their conventional values where those numbers are calculated based on hydraulic diameter. Here we assume that the channel half height, D, is much smaller than the channel width W ($W \gg D$). Therefore,

the flow can be treated as two-dimensional as shown in Fig. 1. For convenience we use two different schemes to normalize the temperature: one for constant surface temperature as $\theta = (T - T_s)/(T_i - T_s)$ and the other one for constant wall heat flux as $\theta = k(T - T_i)/Dq''_s$, where T_s is the channel surface temperature, T_i is the inlet temperature, and q''_s, is the surface heat flux [17]. Therefore, for both boundary conditions, the normalized governing equation becomes

$$Pe_T \frac{\partial \theta}{\partial \xi} = \frac{\partial^2 \theta}{\partial \xi^2} + \frac{\partial^2 \theta}{\partial \eta^2} + G \tag{8}$$

where G is the normalized generation term that represents the ratio of Joule heating to surface heat flux. Since we used two different expressions to normalize the temperature, the normalized source term, G, also has two different forms. For constant wall temperature, G can be expressed as $\sigma(\vec{E}\cdot\vec{E})D^2/k(T_i - T_s)$, and for constant wall heat flux G is presented as $\sigma(\vec{E}\cdot\vec{E})D/q''_s$. In Eq. (8), Pe_T is the thermal Peclet number and can be expressed as

$$Pe_T = Re \cdot Pr = \frac{u_{HS}D}{\nu}\cdot\frac{\nu}{\alpha} = \frac{u_{HS}D}{\alpha}$$

where α is the thermal diffusivity and Pr is the Prandtl number. In this study, we only deal with thermal Peclet number.

4. Thermal analysis

4.1. Isothermal wall condition

In this case, the normalized energy transport equation is subjected to the following boundary conditions

$$\theta(\xi = 0, \eta) = 1 \tag{9a}$$

$$\theta(\xi \to \infty, \eta) < \infty \tag{9b}$$

$$\left.\frac{\partial \theta}{\partial \eta}\right|_{(\xi,\eta=0)} = 0 \tag{9c}$$

$$\theta(\xi, \eta = 1) = 0 \tag{9d}$$

Here, the normalized generation term (G) can be positive or negative depending on the relative magnitude of the inlet temperature, T_i, over the surface temperature, T_s. The generation term, $G = 0$ corresponds to Stokes flow with no Joule heating. If the difference between surface and inlet temperature reaches to zero, the generation term goes to infinity. Therefore, this analysis is particularly valid when inlet temperature is different from surface temperature. We obtain the solution of the normalized temperature from governing equation (8) based on boundary conditions presented by Eqs. (9). Since Eq. (8) is a non-homogenous partial differential equation, we divide it into two components such that the total solution, θ, becomes

$$\theta = \theta_h + \theta_o \tag{10}$$

where θ_h and θ_o are the homogenous and non-homogeneous part of the solution, respectively.

The homogeneous solution is obtained by using the separation of variables technique as [22]

$$\theta_h = \sum_{n=0}^{\infty} \alpha_n \exp\{-\gamma_n \xi\} \cos\left(\sqrt{\lambda_n}\eta\right) \tag{11}$$

where the eigenvalues, λ_n, are given by $\lambda_n = \{(n+\frac{1}{2})\pi\}^2$, the Fourier coefficients, α_n, are calculated as $\alpha_n = \frac{2\cdot(-1)^n}{\sqrt{\lambda_n}}$, and the exponential decay parameter, γ_n, is defined as

$$\lambda_n = \frac{\sqrt{Pe_T^2 + 4\lambda_n} - Pe_T}{2}.$$

On the other hand, the non-homogeneous solution has been found as [23]

$$\theta_o = \sum_{n=0}^{\infty} \left(\frac{\alpha_n \cdot G}{\lambda_n}\right)[1 - \exp\{-\gamma_n \xi\}] \cos\left(\sqrt{\lambda_n}\eta\right) \tag{12}$$

Therefore, the total solution for the non-dimensional temperature distribution becomes

$$\begin{aligned}\theta &= \theta_h + \theta_o \\ &= \frac{G}{2}(1-\eta^2) + \sum_{n=0}^{\infty} \alpha_n \left(1 - \frac{G}{\lambda_n}\right) \exp\{-\gamma_n \xi\} \cos\left(\sqrt{\lambda_n}\eta\right)\end{aligned} \tag{13}$$

where $\sum_{n=0}^{\infty}(\frac{\alpha_n}{\lambda_n})\cos(\sqrt{\lambda_n}\eta)$ can be replaced as $\frac{1}{2}(1-\eta^2)$. At any section of the channel, the normalized bulk mean temperature can be obtained from following expression

$$\theta_m = \frac{T_m - T_s}{T_i - T_s} = \frac{1}{u_m A}\int_{A_C} (\theta u)\, dA \tag{14}$$

where T_m is the mean temperature, u_m is the mean velocity and A_C is the cross-sectional area of the channel ($A_C = 2WD$). Since the flow is plug like in most part of the channel, we can assume $u = u_m \cong u_{HS}$, and the normalized bulk mean temperature becomes

$$\begin{aligned}\theta_m &= \frac{1}{2D}\int_{-D}^{D} \theta\, dy \\ &= \frac{G}{3} + \sum_{n=0}^{\infty}\left(\frac{2}{\lambda_n}\right)\left(1 - \frac{G}{\lambda_n}\right)\exp\{-\gamma_n \xi\}\end{aligned} \tag{15}$$

Hence, for the isothermal boundary condition, the local heat transfer coefficient can be found as

$$\begin{aligned}h_\xi &= \frac{q''_s}{T_s - T_m} \\ &= \frac{k}{D}\frac{G + \sum_{n=0}^{\infty} 2\left(1 - \frac{G}{\lambda_n}\right)\exp\{-\gamma_n \xi\}}{\frac{G}{3} + \sum_{n=0}^{\infty}\frac{2}{\lambda_n}\left(1 - \frac{G}{\lambda_n}\right)\exp\{-\gamma_n \xi\}}\end{aligned} \tag{16}$$

and the corresponding local Nusselt number becomes

$$Nu_\xi = \frac{Dh_\xi}{k} = \frac{G + \sum_{n=0}^{\infty} 2\left(1 - \frac{G}{\lambda_n}\right)\exp\{-\gamma_n \xi\}}{\frac{G}{3} + \sum_{n=0}^{\infty} \frac{2}{\lambda_n}\left(1 - \frac{G}{\lambda_n}\right)\exp\{-\gamma_n \xi\}} \tag{17}$$

4.2. Constant wall flux condition

Here the normalized governing equation (8) is subjected to the following boundary conditions:

$$\theta(\xi = 0, \eta) = 0 \tag{18a}$$

$$\theta(\xi \to \infty, \eta) < \infty \tag{18b}$$

$$\left.\frac{\partial \theta}{\partial \eta}\right|_{(\xi,\eta=0)} = 0 \tag{18c}$$

$$\left.\frac{\partial \theta}{\partial \eta}\right|_{(\xi,\eta=1)} = 1 \tag{18d}$$

In this analysis, heat flux q''_s is positive when thermal energy enters the control volume. Hence the normalized generation term, G, is positive for heat addition into the channel, and G is negative for heat rejection. We varied the normalized generation term, G, between -1 and 1, where $G = -1$, 0, 1 corresponds to Joule heating equal to surface heat removal, no Joule heating, and Joule heating equal to surface heat addition, respectively. For flow of de-ionized (DI) water ($\sigma = 10^{-3}$ S/m) in a 40 μm deep channel with an electric field, $E_x = 250$ V/mm and heat flux, $q''_s = 1200$ W/m^2 will result in $G = 1$.

In constant heat flux case, the boundary conditions presented by Eqs. (18) are not homogeneous. In order to obtain homogeneous boundary conditions at the wall, we decompose the normalized temperature as [23]

$$\theta = \theta_a + \theta_p \tag{19}$$

where θ_a is the auxiliary temperature field and θ_p is a particular type of function that provides homogeneous boundary condition for the auxiliary temperature field. For a particular function, $\theta_p = (1/2)\eta^2$, the resulting governing equation for the auxiliary temperature field becomes

$$Pe_T \frac{\partial \theta_a}{\partial \xi} = \frac{\partial^2 \theta_a}{\partial \xi^2} + \frac{\partial^2 \theta_a}{\partial \eta^2} + [1 + G] \tag{20}$$

and the corresponding boundary conditions for the auxiliary temperature are

$$\theta_a(\xi = 0, \eta) = -\frac{1}{2}\eta^2 \tag{21a}$$

$$\theta_a(\xi \to \infty, \eta) < \infty \tag{21b}$$

$$\left.\frac{\partial \theta_a}{\partial \eta}\right|_{(\xi,\eta=0)} = 0 \tag{21c}$$

$$\left.\frac{\partial \theta_a}{\partial \eta}\right|_{(\xi,\eta=1)} = 0 \tag{21d}$$

Like the constant surface temperature case, now we decompose the governing equation of the auxiliary temperature into two components: one contains the homogeneous part and the other carries the non-homogeneous part so that

$$\theta_a = \theta_h + \theta_o \tag{22}$$

Using the separation of variables technique, we find the homogeneous solution as

$$\theta_h = -\beta_0 - \sum_{n=1}^{\infty} \beta_n \exp\{-\gamma_n \xi\} \cos\left(\sqrt{\lambda_n}\eta\right) \tag{23}$$

where $\lambda_n = (n\pi)^2$, $\gamma_n \equiv \frac{\sqrt{Pe_T^2 + 4\lambda_n} - Pe_T}{2}$, $\beta_0 = \frac{1}{6}$ and $\beta_n = \frac{2(-1)^n}{(n\pi)^2}$.

The non-homogeneous solution becomes, $\theta_o = \left(\frac{1+G}{Pe_T}\right)\xi$. Therefore the total solution for the normalized temperature distribution in constant wall heat flux can be written as

$$\begin{aligned}\theta &= \theta_p + \theta_h + \theta_o \\ &= \left(\frac{1+G}{Pe_T}\right)\xi + \sum_{n=1}^{\infty} \beta_n [1 - \exp\{-\gamma_n \xi\}] \cos\left(\sqrt{\lambda_n}\eta\right)\end{aligned} \tag{24}$$

where $\theta_p = \frac{1}{2}\eta^2 = \beta_0 + \sum_{n=1}^{\infty} \beta_n \cos(\sqrt{\lambda_n}\eta)$. Hence the normalized surface temperature becomes

$$\theta_s = \left(\frac{1+G}{Pe}\right)\xi + \sum_{n=1}^{\infty} \frac{2}{\lambda_n}[1 - \exp\{-\gamma_n \xi\}] \tag{25}$$

For plug like electroosmotic flow velocity, the normalized bulk mean temperature can be found as

$$\theta_m = \frac{1}{u_m A}\int_{A_C} (\theta u)\mathrm{d}A = \frac{1}{2D}\int_{-D}^{D} \theta \,\mathrm{d}y = \left(\frac{1+G}{Pe}\right)\xi \tag{26}$$

Therefore, the local heat transfer coefficient can be obtained as

$$h_\xi = \frac{q''_s}{T_s - T_m} = \frac{k}{D}\frac{1}{\sum_{n=1}^{\infty} \frac{2}{\lambda_n}[1 - \exp\{-\gamma_n \xi\}]} \tag{27}$$

and the corresponding local Nusselt number becomes

$$Nu_\xi = \frac{h_\xi D}{k} = \frac{1}{\sum_{n=1}^{\infty} \frac{2}{\lambda_n}[1 - \exp\{-\gamma_n \xi\}]} \tag{28}$$

5. Discussion of results

For both isothermal and constant surface heat flux channel surface thermal conditions, the analytical solutions for local temperature, wall temperature, bulk mean temperature, local heat transfer coefficient, and local Nusselt number are obtained in terms of infinite series

solutions as presented by Eqs. (13)–(17) and (24)–(27). Numerical techniques are used to find the convergence results for the above-mentioned parameters with an accuracy of 99.99% by summing at least 1000 terms of the infinite series. In the absence of any special functions, convergence of the series was straightforward without any numerical difficulty. Analytical solutions are presented for DI water for $Re < 1$, $Pr = 7$, and $D > 1000\lambda$. Therefore, the hydrodynamic entry length is negligible, and the uniform "plug-like" velocity is justified from the very beginning of the channel.

5.1. Isothermal wall condition

The normalized fluid temperature distribution, θ, across the channel is shown in Fig. 2 at different axial locations for Peclet number, $Pe_T = 1$. Due to the symmetric hydrodynamic and thermal boundary conditions, we have plotted temperature distributions for the upper half of the channel. Although the analytical result obtained in Eq. (13) is valid for any finite value of the normalized source term (G), we have presented the temperature distribution for only three different source term values ($G = -1$, 0, 1).

Fig. 2(a) shows the temperature development along the channel for a dimensionless source term $G = -1$. For the negative value of the non-dimensional source term, the channel surface temperature is higher than the inlet temperature of fluid ($T_s > T_i$). The normalized temperature becomes zero at the surface ($\eta = 1$) to conserve the isothermal boundary condition at the wall. At the entry, the fluid temperature is very close to the inlet temperature, and the normalized temperature becomes unity across the channel. In the entry region, since the surface temperature is higher than the fluid temperature, the heat flux enters into the channel for $G = -1$. However, as the fluid travels along the channel, the normalized fluid temperature (θ) and the wall heat flux decrease, but the dimensional fluid temperature (T) increase due to Joule heating.

Further down the channel, both normalized fluid temperature and wall heat flux become negative, and the temperature profile does not change anymore on or after $\xi = 10$. Therefore, we obtain thermally fully developed region within 10 characteristic dimensions from the entry. In the fully developed region, the thermal energy leaving through the boundary is equal to the heat generated by the Joule heating.

Fig. 2(b) shows the normalized temperature distribution for the negligible or no Joule heating case. This is a classical heat transfer situation where a fully developed flow with uniform (slug flow) velocity passes through a 2-D isothermal microchannel. Although Joule heating always exists in the electroosmotic flow, we presented that in order to compare with the existing literature. In this case, the normalized temperature decreases along the channel as fluid travels towards the downstream direction. However, the non-dimensional temperature never goes beyond zero, and both fluid and surface temperature reach the same value by the 10 channel

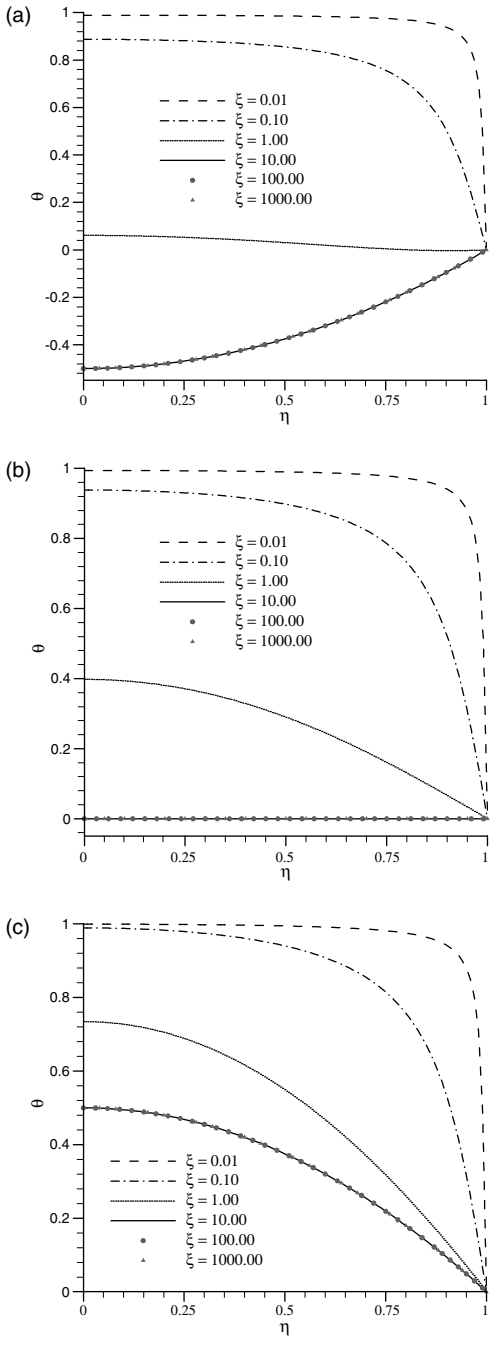

Fig. 2. Non-dimensional temperature, θ, distribution across the channel in pure electroosmotic flow at different downstream locations, ξ, for both walls subjected to isothermal conditions at $Pe_T = 1.0$ for (a) $G = -1$, (b) $G = 0$, and (c) $G = 1$.

characteristic dimension from the inlet, $\xi = 10$. Without internal heat generation, the heat transfer between the channel and environment takes place only in the entry region. In the entry region, the net wall heat flux is positive or negative, depending on the relative magnitude of fluid inlet temperature, T_i, over surface temperature, T_s. On the other hand, the rest of the channel has no temperature change.

The normalized temperature distribution across the channel for the positive source term, $G = 1$, is presented in Fig. 2(c). In this case, the fluid inlet temperature is higher than the channel surface temperature ($T_i > T_s$). Unlike the negative source term ($G = -1$), the normalized temperature (θ) is always positive. Therefore, fluid temperature for this case is always higher than the channel surface temperature. Here both local fluid temperature and heat flux decrease as the flow progresses, but they do not change after reaching $\xi = 10$. After that, the amount of heat rejected from the channel is balanced with the volumetric thermal energy generation due to Joule heating.

Fig. 3 shows the local Nusselt number distribution along the channel for all three cases ($G = -1$, 0, and 1) presented in Fig. 2 for $Pe_T \leqslant 5$. Since the local Nusselt number is the same for each case after reaching the fully developed condition, they have been presented up to $\xi = 10$. For isothermal channel surface condition, the Nusselt number is very high at the entry point, but it decays abruptly to reach a flat value within one characteristic length (D). The local Nusselt number distribution along the channel also identifies the exact location where the flow is thermally fully developed. The fully developed Nusselt number is independent of the Peclet number in the electroosmotically driven slug flow region, but it depends on the magnitude of the source term as shown in Fig. 3. For both positive and negative source terms considered in this study ($G = 1$ and -1), the Nusselt number reaches a value of 3.0 in the fully developed region. On the other hand, without Joule heating the heat transfer characteristics are identical to the classical isothermal heat transfer in a slug flow, for which the fully developed Nusselt number is 2.467 [18].

5.2. Constant wall flux condition

Analytical solution for normalized temperature, θ, distribution within the channel is presented in Eq. (24), and the corresponding wall temperature distribution is given in Eq. (25). The first *linear* term of Eq. (24) shows the temperature variation only on the streamwise direction, while the second term has contribution from both streamwise and cross-stream directions. In Fig. 4, we show the normalized wall temperature (θ_s) distribution along the channel for three different values of generation term, though our analytical results are valid for any value of non-dimensional generation term, G. Here

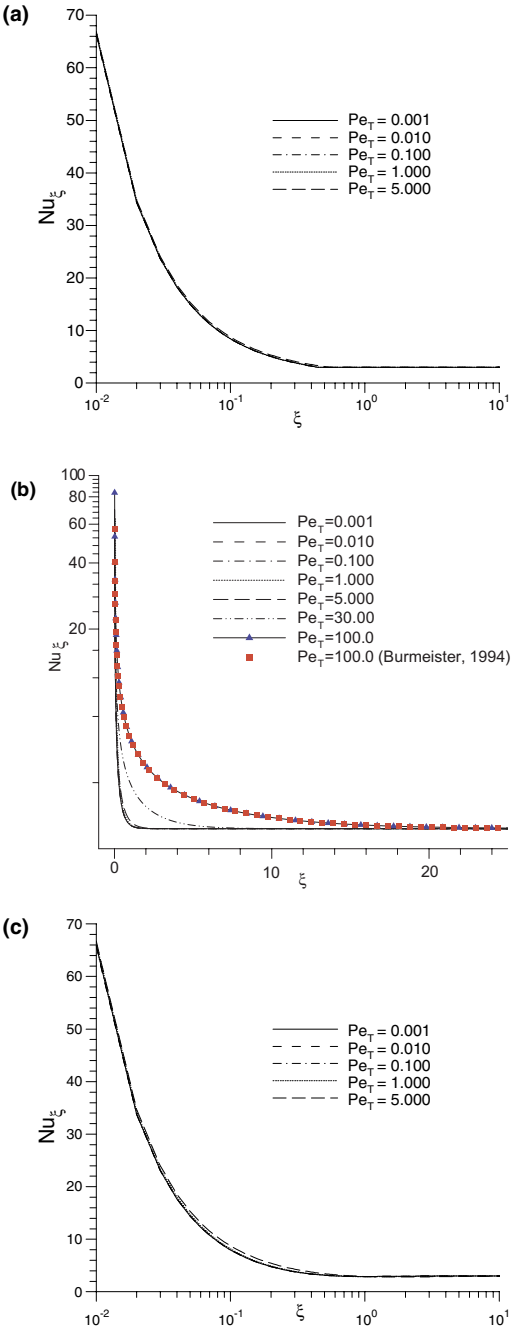

Fig. 3. Local Nusselt number distribution for both walls subjected to isothermal boundary conditions under various Peclet number for (a) $G = -1$, (b) $G = 0$, and (c) $G = 1$. The fully developed Nusselt number for case (a) or (c) is 3.0. For no Joule heating (Case b), our analytical solutions exactly match existing results [17,18], and the fully developed Nusselt number for this case is 2.467.

the *linear* first term, in normalized wall temperature distribution (Eq. (25)), causes a monotonic temperature

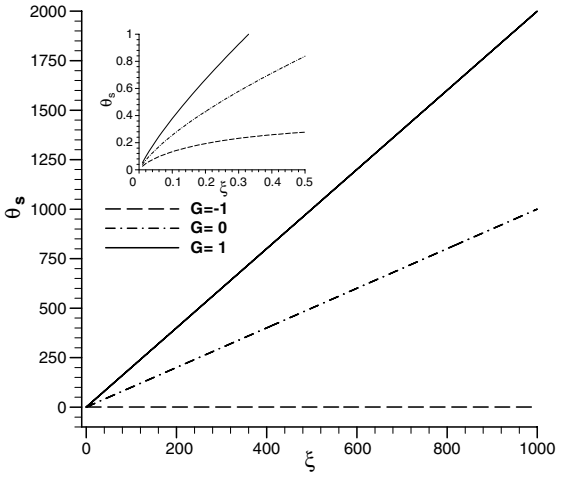

Fig. 4. Normalized wall temperature, θ_s, distribution along the channel in pure electroosmotic flow for both walls subjected constant heat flux boundary conditions at $Pe_T = 1.0$ for different normalized source terms. Onset figure shows the variation of wall temperature at the entry region.

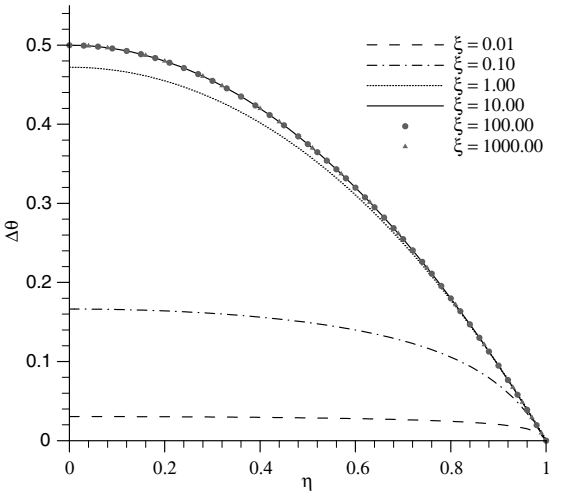

Fig. 5. Non-dimensional temperature difference, $\Delta\theta = \theta_s - \theta$, across the channel in pure electroosmotic flow at different downstream locations, ξ, for both walls subjected to constant wall heat flux at $Pe_T = 1.0$.

change with axial location for any value of G, except for $G = -1$ case. For $G = -1$, the amount of Joule heating is equal to the surface heat rejection, and hence the dimensional wall temperature (T_s) reaches a constant value after the thermal entry region. Although non-dimensional wall temperature can change a couple of orders of magnitude in the downstream direction (for $G \neq -1$), the dimensional temperature change, $(T_s - T_i)$ is less than 5 K due to the conversion factor $q''_s D/k = 5 \times 10^{-4}$ K, even for an external electric field, $\vec{E} = 100$ V/mm and electrical conductivity, 300 μS/m in a 20 μm deep channel. Therefore, temperature independence on fluid properties can be justified at any section of the channel.

The normalized temperature difference, $\Delta\theta = \theta_s - \theta$, distribution across the channel is plotted in Fig. 5 at different axial locations for $Pe_T = 1$. The general trends of normalized temperature difference, $\Delta\theta$, distribution remain same for any value of G. The temperature distribution is almost uniform at the beginning of the channel ($\xi \to 0.0$), and the corresponding fluid temperature is very close to inlet temperature, T_i. As the flow proceeds along the channel, the non-dimensional temperature difference ($\Delta\theta$) increases, especially at the centerline, until it reaches a constant value of 0.5 at the centerline. Fig. 5 indicates that there is no change of $\Delta\theta$ distribution across the channel after ten characteristic dimensions from the entrance, $\xi = 10$. However, the dimensional temperature, $T(x, y)$, distribution changes along the channel since the wall temperature, $T_s(x)$, varies in the downstream direction. In following section, we discuss the dimensional temperature distribution for three different normalized generation terms ($G = -1$, 0, and 1).

For $G = -1$ case, the heat is taken away from the channel by external means ($q''_s < 0$), and there is no change in the wall temperature after the thermally developing region (refer to Fig. 4). Therefore the dimensional fluid temperature (T) is higher than the channel surface temperature (T_s), although the non-dimensional temperature difference, $\Delta\theta$, is positive within the fluid. On the other hand, in case of positive source term ($G = 1$), both heat generation and heat addition take place simultaneously. As expected, both surface and centerline temperature increase as the flow proceeds along the downstream direction, and the surface temperature is always higher than centerline temperature.

The no Joule heating case ($G = 0$) is very similar to classical heat transfer study for constant surface heat flux without any generation. There could be two possible scenarios: heat rejection from the channel and heat addition to the channel. For heat rejection from the channel, both dimensional surface and centerline temperatures decrease. On the other hand, for heat addition both dimensional surface and centerline temperature increase. From Fig. 5, it is clear that the dimensional surface temperature is higher than the fluid temperature, if heat is added in the system, and vice versa. We also obtained temperature distribution (not presented here) at high Peclet number flows for $G = 0$, and our results replicate the existing analytical work [17,18].

The mean temperature, which is presented by Eq. (26), shows only linear dependence on axial positions. However, the difference between non-dimensional surface and mean temperature, $(\theta_s - \theta_m)$, is independent of the source term G. Therefore, in the fully developed

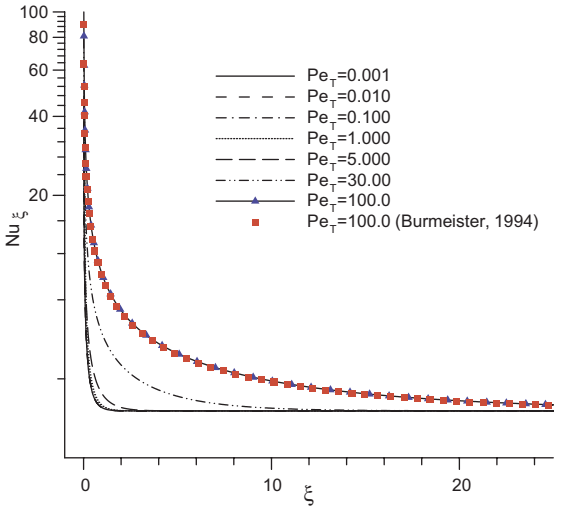

Fig. 6. Local Nusselt number distribution under various Peclet number for both walls subjected to constant heat flux boundary conditions. At high Peclet numbers our results exactly match the existing results [17,18]. The fully developed Nusselt number for constant wall heat flux case is 3.01.

region we obtain identical heat transfer coefficient and Nusselt number for any value of Joule heating and external heat flux. Fig. 6 shows the local Nusselt number distribution along the channel for different values of the Peclet number. Within the microflow regime considered in this study, the heat transfer characteristics are independent of the flow Reynolds number, except in the developing region where the Nusselt number is very high. From Fig. 6, it is clear that the flow is thermally fully developed within five characteristic dimension from the entrance, $\xi = 5$, and the corresponding Nusselt number for this case is 3.01. Therefore the Nusselt number in the fully developed region is within 1% of that of fully developed uniform flow with no Joule heating case reported earlier [17,18].

6. Summary and conclusions

We obtained analytical solutions for heat transfer characteristics of electroosmotically driven Newtonian fluid in two-dimensional straight microchannels for constant zeta potential, buffer concentration, and external electric field. The energy equation for electroosmotically originated flows have been analyzed for both constant surface temperature and constant wall heat flux thermal boundary conditions in the presence of significant Joule heating. This analysis is based on *infinitesimal* Debye length ($\lambda/D \geqslant 1000$), and hence a plug like uniform velocity profile is assumed throughout the channel. Our analysis resulted in the following:

- In electroosmotically driven microchannel flows, the Joule heating contribution is important if the channel thickness is higher than 20 μm.
- For isothermal channel surface condition, the local fluid temperature decreases for positive source term ($G > 0$) and increases for negative source term ($G < 0$), along the channel, before it reaches an identical profile. Although both local and mean (normalized) temperature is a function of the source term, the normalized heat transfer coefficient reaches the same value for both positive and negative source terms as long as the magnitude of G is the same.
- In constant surface heat flux condition, the local fluid temperature increases monotonically along the channel for positive and no source term ($G \geqslant 0$). But for the negative source term ($G < 0$), the local fluid temperature may increase or decrease depending on the relative values of G.
- For surface heat flux case, the Nusselt number does not depend on the magnitude of the source term.
- Under no Joule heating case, our results verify the Nusselt number of classical slug flows in 2-D channels.
- Within the thermally fully developed region, the local Nusselt number is independent of the Peclet number for the electroosmotic microflow region considered in this study.

Acknowledgements

The authors thank Dr. Hong-Ming Yin for his valuable suggestions. This investigation was supported in part by funds provided by the Washington State University Office of Research.

References

[1] F.F. Reuss, Charge-induced flow, Proceedings of the Imperial Society of Naturalists of Moscow 3 (1809) 327–344.
[2] G. Wiedemann, Pogg. Ann. 87 (1852) 321.
[3] P.H. Paul, M.G. Garguilo, D.J. Rakestraw, Imaging of pressure and electrokinetically driven flows through open capillaries, Anal. Chem. 70 (1998) 2459–2467.
[4] S. Zeng, C.H. Chen, J.C. Mikkelsen, J.G. Santiago, Fabrication and characterization of electroosmotic micropumps, Sensor. Actuator. B Chem. 79 (2001) 107–114.
[5] S. Zeng, C.H. Chen, J.G. Santiago, J.R. Chen, R.N. Zare, J.A. Tripp, F. Svec, J.M.J. Frechet, Electroosmotic flow pumps with polymer frits, Sensor. Actuator. B Chem. 82 (2002) 209–212.
[6] A.M. Leach, A.R. Wheeler, R.N. Zare, Flow injection analysis in a microfluidic format, Anal. Chem. 75 (2003) 967–972.

[7] B.S. Broyles, S.C. Jacobson, J.M. Ramsey, Sample filteration, concentration, and separation integrated on microfluidic devices, Anal. Chem. 75 (2003) 2761–2767.
[8] D. Burgreen, F.R. Nakache, Electrokinetic flow in ultrafine capillary slits, J. Phys. Chem. 68 (1964) 1084–1091.
[9] C.L. Rice, R.J. Whitehead, Electrokinetic flow in a narrow cylindrical capillary, J. Phys. Chem. 69 (1965) 4017–4023.
[10] P. Dutta, A. Beskok, Analytical solution of combined electroosmotic/pressure driven flows in two-dimensional straight channels: finite Debye layer effects, Anal. Chem. 73 (2001) 1979–1986.
[11] J.G. Santiago, Electroosmotic flows in microchannels with finite inertial and pressure forces, Anal. Chem. 73 (2001) 2353–2365.
[12] A.E. Herr, J.I. Molho, J.G. Santiago, M.G. Mungal, T.W. Kenny,, M.G. Garguilo, Electroosmotic capillary flow with non-uniform zeta potential, Anal. Chem. 72 (2000) 1053–1057.
[13] C.H. Chen, J.G. Santiago, A planar electroosmotic micropump, J. Micro-electromech. Syst. 11 (6) (2002) 523–528.
[14] K. Swinney, D.J. Bornhop, Quantification and evaluation of Joule heating in on-chip capillary electrophoresis, Electrophoresis 23 (2002) 613–620.
[15] W.A. Gobie, C.F. Ivory, Thermal model of capillary electrophoresis and a method of counteracting thermal band broadening, J. Chromatography 516 (1990) 191–210.
[16] E.M. Sparrow, J.L. Novotny, S.H. Lin, Laminar flow of a heat-generating fluid in a parallel-plate channel, AIChE J. 9 (6) (1963) 797–804.
[17] W.M. Kays, M.E. Crawford, Convective Heat and Mass Transfer, third ed., McGraw-Hill Book, New York, 1993.
[18] L.C. Burmister, Convective Heat Transfer, Wiley, New York, 1994.
[19] D. Maynes, B.W. Webb, Fully developed electro-osmotic heat transfer in microchannels, Int. J. Heat Mass Transfer 46 (2003) 1359–1369.
[20] R.F. Probstein, Physiochemical Hydrodynamics: An Introduction, Wiley, New York, 1994.
[21] R.J. Hunter, Zeta Potential in Colloid Science: Principles and Applications, Academic Press, New York, 1981.
[22] R. Haberman, Elementary Applied Partial Differential Equations: with Fourier Series and Boundary Conditions, third ed., Prentice-Hall, Upper Saddle River, NJ, 1998.
[23] M.A. Pinsky, Partial Differential Equations and Boundary-Value Problems with Applications, third ed., McGraw-Hill, Columbus, OH, 1998.